Article

Discovery Medicine 2026; 38(214): 3610–3623
https://doi.org/10.24976/Discov.Med.202638214.275

EP300 Enhances Malignant Phenotypes of CAL-27 Cells in Association With JAK2/STAT3 Activation and an M2-Associated Macrophage Phenotype

Weiwei He[1,*], Sai Ma[1], Weilong Lin[1], Jiashuo Yang[1]

[1]Department of Stomatology, The First Affiliated Hospital of Hebei North University, 075000 Zhangjiakou, Hebei, China
*Correspondence: gege13993@126.com (Weiwei He)
Submitted: 10 August 2026 Revised: 7 September 2026 Accepted: 23 September 2026 Published: 25 November 2026

Background: Oral squamous cell carcinoma (OSCC) is characterized by local invasion and an immunosuppressive microenvironment dominated by M2-skewed tumor-associated macrophages. EP300 encodes the acetyltransferase p300, which has been reported to acetylate signal transducer and activator of transcription 3 (STAT3); however, whether tumor-cell EP300 abundance is associated with JAK2/STAT3 activation and macrophage skewing in OSCC remains unclear.

Methods: EP300 expression was compared between CAL-27 OSCC cells and normal human oral keratinocytes (HOK). Stable shRNA knockdown and transient overexpression were established in CAL-27 cells. JAK2 and STAT3 activation was assessed based on phosphorylated-to-total ratios. Cell viability, migration and invasion were measured using CCK-8 and Transwell assays, with the STAT3 inhibitor Stattic used for rescue experiments. Phorbol 12-myristate 13-acetate (PMA)-differentiated THP-1 macrophages were exposed to conditioned medium collected from donor cultures at matched confluence and assessed for CD163, Arg-1, CD86 and p-STAT3 expression. Knockdown was further evaluated in nude mouse xenografts (female BALB/c, n = 5 per group) by immunohistochemistry.

Results: EP300 mRNA and protein were higher in CAL-27 cells than in HOK cells (both $p < 0.001$). EP300 silencing reduced the p-JAK2/JAK2 and p-STAT3/STAT3 ratios, whereas overexpression increased both ratios (all $p < 0.01$). OE-EP300 increased viability and the number of migrated and invaded cells (all $p < 0.001$), and each effect was reversed by Stattic (all $p < 0.01$ vs OE-EP300 + DMSO). Conditioned medium from OE-EP300 cells increased CD163, Arg-1 and p-STAT3 in macrophages, whereas conditioned medium from shEP300 cells decreased their expression (all $p < 0.001$); CD86 expression remained unchanged across groups ($p > 0.05$). Co-treatment with Stattic lowered macrophage p-STAT3 and abolished the induction of CD163 and Arg-1 (all $p < 0.001$). *In vivo*, shEP300 tumors showed reduced volume and weight, accompanied by decreased EP300, Ki-67, CD163 and p-STAT3 immunoreactivity (all $p < 0.001$).

Conclusions: EP300 abundance is associated with JAK2/STAT3 activation and a more aggressive phenotype in CAL-27 cells, and EP300-overexpressing cells promote M2-associated marker expression in human macrophages through soluble factors, an effect that was reversed by pharmacological inhibition of STAT3. The responsible mediator was not identified, the contribution of EP300-driven changes in donor-cell proliferation to conditioned-medium composition was not formally excluded, and validation in immunocompetent models is required.

Keywords: oral squamous cell carcinoma; EP300/p300; JAK2/STAT3 signaling; tumor-associated macrophages; M2-associated phenotype

Introduction

Oral squamous cell carcinoma (OSCC) represents the predominant histological form of malignancy arising in the oral cavity, accounting for approximately 90% of oral malignancies [1]. Although surgery, radiotherapy and systemic treatment have improved disease management, local invasion, cervical lymph-node involvement and recurrence continue to limit long-term disease control [2,3,4]. Genomic analyses have identified recurrent alterations in tumor suppressors, oncogenic pathways and chromatin regulators in head and neck squamous cell carcinoma [5,6,7]. However, tumor-cell-intrinsic abnormalities alone do not fully account for the biological diversity of OSCC [8,9]. Increasing evidence indicates that interactions between malignant epithelial cells and the surrounding stromal and immune compartments substantially contribute to tumor growth and dissemination [10,11,12,13].

Tumor-associated macrophages represent a prominent and functionally plastic component of the OSCC microenvironment [14]. Clinical studies have associated increased densities of CD163-positive macrophages, particularly within the tumor stroma, with lymph node metastasis and unfavorable clinical outcomes [15,16,17]. Macrophage

Copyright: © 2026 The Author(s). Published by Discovery Medicine. This is an open access article under the CC BY 4.0 license.
Note: *Discovery Medicine* stays neutral with regard to jurisdictional claims in published maps and institutional affiliations.

phenotypes are commonly described along an M1–M2 spectrum, with M2-associated states generally linked to tissue remodeling, angiogenesis and immune regulation [18,19]. Nevertheless, macrophages in human tumors rarely conform to a strictly binary classification and may co-express markers associated with different activation programs [20,21]. Accordingly, changes in markers such as CD163, CD206, Arg-1 or CD86 should be interpreted as evidence of phenotypic skewing rather than as definitive assignment to a fixed macrophage subtype.

The phenotype of tumor-infiltrating macrophages is shaped in part by soluble mediators released from malignant cells [22,23]. The resulting macrophage states, in turn, release cytokines and extracellular vesicles that reinforce OSCC-cell growth, survival, stemness, and motility while suppressing antitumor immune responses, thereby establishing reciprocal paracrine circuits [24,25]. Signal transducer and activator of transcription 3 (STAT3) represents a potential signaling convergence point in the bidirectional crosstalk between OSCC cells and tumor-associated macrophages [24,26]. Following activation by upstream Janus kinases and other tyrosine kinases, STAT3 regulates genes involved in cell survival, migration and inflammatory signaling [27,28]. Tumor-derived signals can also activate STAT3 in macrophages and promote the expression of immunoregulatory and M2-associated molecules [26,29]. Thus, molecular regulators capable of modifying STAT3 activity and the tumor-cell secretome may influence both the malignant phenotype and the composition of the surrounding immune microenvironment.

EP300 encodes the transcriptional coactivator p300, which possesses intrinsic lysine acetyltransferase activity and regulates chromatin accessibility, enhancer activity and the function of numerous transcription factors [30]. The biological effects of EP300 are context-dependent, and both loss-of-function alterations and tumor-supportive activities have been described across different malignancies [31]. In OSCC models, previous studies have implicated EP300 in invasion, glycolytic regulation and Notch-related cellular programs [32,33]. In addition, p300 can acetylate STAT3 at Lys685, a modification reported to facilitate STAT3 dimerization, DNA binding and transcriptional activity [34]. These observations provide a plausible basis for functional interaction between EP300 and STAT3 signaling. Nevertheless, whether changes in tumor-cell EP300 abundance are associated with JAK2/STAT3 activation in OSCC, and whether EP300-expressing tumor cells influence macrophage phenotype through paracrine signaling, remain incompletely understood.

In the present study, we examined the effects of EP300 knockdown and overexpression on JAK2/STAT3 phosphorylation and malignant phenotypes in CAL-27 OSCC cells. Conditioned medium experiments were used to determine whether altering EP300 expression in tumor cells affected M2-associated marker expression in THP-1-derived macrophages. We further assessed whether pharmacological inhibition of STAT3 attenuated the tumor cell and macrophage responses associated with EP300 overexpression. A subcutaneous xenograft model was also employed to investigate whether EP300 knockdown altered tumor growth, STAT3 activation and CD163 immunoreactivity *in vivo*. These experiments were designed to evaluate a potential EP300-associated tumor-macrophage signaling relationship while avoiding assumptions regarding a direct molecular interaction or the identity of the responsible soluble mediator.

Materials and Methods

Cell Lines and Culture

CAL-27 (human OSCC, CRL-2095) and THP-1 (human monocytic leukemia, TIB-202) cells were sourced from American Type Culture Collection (Manassas, VA, USA). Human oral keratinocytes (HOK) cells were obtained from ScienCell Research Laboratories (2610, Carlsbad, CA, USA). CAL-27 cultures were incubated in DMEM (PM150210, Procell, Wuhan, China) containing 10% fetal bovine serum (FBS; FSP500, ExCell Bio, Suzhou, China) and 1% penicillin-streptomycin (C0222, Beyotime, Shanghai, China), while THP-1 cells were maintained in RPMI-1640 (PM150110, Procell, Wuhan, China) supplemented with the same concentrations of FBS and penicillin-streptomycin plus 0.05 mM 2-mercaptoethanol (M3148, Sigma-Aldrich, St. Louis, MO, USA). HOK cells were cultured in oral keratinocyte medium (2611, ScienCell, Carlsbad, CA, USA) supplemented as specified by the supplier. Incubation throughout was at 37 °C under 5% CO_2 with saturated humidity. All lines tested negative for mycoplasma and were verified by short tandem repeat profiling.

EP300 Knockdown and Overexpression

EP300 silencing was achieved using a lentiviral shRNA construct (shEP300, targeting 5′-CGCTTGTATCTCCGAAAGAATTA-3′), with a scrambled sequence (shNC, 5′-CCGGCAACAAGATGAAGAGCACCAACTCGAGTTGGTGCTCTTCATCTTGTTGTTTTT-3′) used as the control. Both constructs were cloned into the pLKO.1-puro backbone (JY10011, Jiangyuan Biotechnology, Nanjing, China). Viral particles generated in HEK-293T cells (CL-0005, Procell, Wuhan, China) were applied to CAL-27 monolayers together with 8 μg/mL polybrene (C0351, Beyotime, Shanghai, China) at an MOI of 20, after which stably transduced populations were obtained by 5-day selection in 1 μg/mL puromycin (ST551, Beyotime, Shanghai, China).

Gain-of-function experiments were achieved by inserting the full-length human EP300 coding sequence (NCBI Reference Sequence NM_001429.4, encoding 2414 amino acids) into pcDNA3.1 (V79020, Invitrogen, Waltham, MA, USA) to generate OE-EP300, with the

empty vector used as the matched control. The reading frame and orientation of the insert were confirmed across the entire coding region by bidirectional Sanger sequencing before use. CAL-27 cells at approximately 70–80% confluence in six-well plates were transfected with the constructs using Lipofectamine 3000 (L3000015, Thermo Fisher Scientific, Waltham, MA, USA) and collected 48 h later. The efficacy of both manipulations was verified at the mRNA and protein levels before any downstream assay was performed.

Quantitative Real-Time PCR

The RNA simple Total RNA Kit (DP424, TIANGEN, Beijing, China) was used for total RNA extraction, and first-strand synthesis was performed using the SweScript All-in-One RT SuperMix for qPCR (G3337, Servicebio, Wuhan, China). Amplification was monitored using a LightCycler96 PCR instrument (Roche, Mannheim, Germany) with SYBR Green master mix (FP205, TIANGEN, Beijing, China), and each sample was analyzed in technical triplicate. Primers were EP300, 5′-TGCCAAACCAGATGATGCCT-3′ (forward) and 5′-TACAGCTGGCTGGGAAAGTG-3′ (reverse), and GAPDH, 5′-TTTTGCGTCGCCAGCC-3′ (forward) and 5′-ATGGAATTTGCCATGGGTGGA-3′ (reverse). Transcript abundance was normalized to GAPDH and calculated as the fold change using the $2^{-\Delta\Delta Ct}$ method.

Western Blotting

Whole-cell lysates were prepared in RIPA buffer (P0013J, Beyotime, Shanghai, China) supplemented with protease and phosphatase inhibitors (ST506, Beyotime, Shanghai, China), and then clarified by centrifugation at 12,000 ×g for 15 min at 4 °C. Protein concentrations were determined using a BCA assay (P0012S, Beyotime, Shanghai, China), and 20–30 µg of protein per lane was separated by 10% SDS-PAGE gels (P0015, Beyotime, Shanghai, China) and electrotransferred onto PVDF membranes (IPVH00010, Millipore, Burlington, MA, USA). Membranes were blocked for 1 h at room temperature in TBST containing 5% skimmed milk, with 5% BSA used instead when probing for phospho-epitopes. The membranes were then incubated overnight at 4 °C with primary antibodies. The antibodies used, with dilutions, included EP300 (1:5000, HA723736, HUABIO, Woburn, MA, USA), p-JAK2 Tyr1007/1008 (1:1000, AF3764, Affinity Biosciences, Jiangsu, China), JAK2 (1:2000, M1501-8, HUABIO), p-STAT3 Tyr705 (1:1000, ET1607-39, HUABIO), STAT3 (1:2000, ET1605-45, HUABIO), CD163 (1:5000, HA724034, HUABIO), Arg-1 (1:1000, HA723143, HUABIO), CD86 (1:5000, ET1606-50, HUABIO) and GAPDH (1:5000, 60004-1-Ig, Proteintech, Rosemont, IL, USA). A 1-h room-temperature incubation with HRP-linked secondary antibody (1:2000, ZB-2301/2305, ZS Golden Bridge, Beijing, China) followed by three TBST washes. Signals were captured on a Tanon-4600 chemiluminescence imaging system (Tanon Science & Technology, Shanghai, China) after enhanced chemiluminescence (P0018S, Beyotime, Shanghai, China) development. Densitometric analysis was performed using ImageJ (version 1.54b, National Institutes of Health, Bethesda, MD, USA) to normalize total protein levels to GAPDH, whereas JAK2 and STAT3 activation was expressed as the ratio of phosphorylated to total protein. In addition, total JAK2 and total STAT3 were quantified relative to GAPDH in the same lanes, and these values are presented in the statistical graphs alongside the phosphorylated-to-total ratios, so that a change in phosphorylation can be distinguished from a change in total protein abundance.

Cell Viability Assay

Suspensions of 3×10^3 cells in 100 µL of complete medium were seeded into 96-well plates and allowed to attach overnight. Forty-eight hours after plating, each well received 10 µL of CCK-8 reagent (MA0218-5, Meilunbio, Dalian, China) and was returned to the incubator for an additional 2 h before absorbance was read at 450 nm (CMax Plus, Molecular Devices, San Jose, CA, USA). Cell-free wells containing medium and reagent were used as the blank.

Transwell Migration and Invasion Assays

Migration was assessed using 24-well inserts with 8-µm polycarbonate membranes (TCS-003-024, BIOFIL, Guangzhou, China). Following 12 h of serum deprivation, 5×10^4 cells suspended in 200 µL of serum-free medium were loaded into the upper compartment. The lower compartment contained 600 µL of medium supplemented with 10% FBS as a chemoattractant. Twenty-four hours later, cells remaining on the upper surface of the membrane were removed with a cotton swab, whereas those that had migrated through the membrane were fixed with 4% paraformaldehyde (G1101, Servicebio, Wuhan, China) for 15 min and then stained with 0.1% crystal violet (C0121, Beyotime, Shanghai, China) for 15 min.

The invasion protocol differed in only two respects. The membranes were pre-coated with Matrigel (356231, Corning, Bedford, MA, USA), diluted 1:8 in serum-free medium, and the incubation period was extended to 48 h. Five randomly selected fields per insert were imaged at 200× magnification using an inverted light microscope (CKX53, OLYMPUS, Tokyo, Japan), and the mean value across the five fields was used for subsequent analysis.

STAT3 Inhibition

A stock of Stattic (HY-13818, MedChemExpress, Monmouth Junction, NJ, USA) was prepared in DMSO (ST038, Beyotime, Shanghai, China) and diluted with culture medium to a final concentration of 5 µM immediately before use. Vehicle controls received an equivalent volume

of DMSO, and the final DMSO concentration did not exceed 0.1% in any well. In the OSCC arm, OE-EP300 CAL-27 cells were exposed to Stattic or vehicle for 2 h before each assay, with the compound retained throughout the assay. In the macrophage arm, Stattic or vehicle was introduced simultaneously with the conditioned medium. Western blotting for p-STAT3 and total STAT3 served to assess the degree of inhibition achieved.

THP-1 Differentiation and Conditioned Medium Treatment

THP-1 monocytes plated at 1×10^6 per well in a six-well format were converted to M0 macrophages by a 24-h exposure to 100 ng/mL phorbol 12-myristate 13-acetate (PMA; HY-18739, MedChemExpress, Monmouth Junction, NJ, USA). The stimulus was then withdrawn, the monolayers were rinsed twice with PBS, and the cells were cultured for a further 24 h in PMA-free medium to allow them to return to a resting state before marker expression was assessed.

Conditioned medium (CM) was prepared from CAL-27 cultures of the shNC, shEP300, vector and OE-EP300 groups. Because EP300 manipulation alters CAL-27 proliferation, seeding densities and seeding times were staggered so that CM collection began only after all four groups had independently reached approximately 80% confluence. Thus, donor cultures were matched for confluence rather than allowed to differ in cell number at the time of collection. The monolayers were then washed twice with PBS and supplied with 2 mL of fresh medium per well, and the supernatant was harvested after a fixed interval of 24 h. Cellular debris was pelleted by centrifugation at 1000 ×g for 5 min, and the supernatant was passed through a 0.22-µm filter (SLGP033RB, Merck Millipore, Burlington, MA, USA). The resulting filtrate was then combined with an equal volume of fresh complete medium immediately before application to macrophages. All groups within a given experiment were prepared, filtered and applied in parallel on the same day.

Rested macrophages were maintained in the respective conditioned medium for 24 h. A parallel well was treated for the same interval with recombinant human IL-4 and IL-13 (20 ng/mL each; 200-04 and 200-13, respectively; PeproTech, Cranbury, NJ, USA), which served as the canonical M2-inducing stimulus. The rescue arm comprised three conditions, including vector CM with vehicle, OE-EP300 CM with vehicle, and OE-EP300 CM with 5 µM Stattic. Lysates from all groups were analyzed by Western blotting for CD163, Arg-1, CD86, p-STAT3 and STAT3.

Subcutaneous Xenograft Model

Six-week-old female BALB/c nude mice weighing 18–20 g were obtained from Vital River (Beijing, China). Mice were housed five per individually ventilated cage under specific pathogen-free conditions at 22 ± 2 °C and 50 ± 10% relative humidity on a 12-h light/dark cycle, with food and water available ad libitum. Animals were acclimatized for 7 days before any procedure. A total of ten mice were used. No animals were used in preliminary experiments. All animal experiments were reviewed and approved by the Experimental Animal Welfare and Ethics Committee of Hebei North University (approval No. HBNU20240622143, approved on 17 June 2024). All procedures were performed in accordance with the institutional guidelines and with the National Standard of the People's Republic of China GB/T 35892-2018 (Laboratory Animal-Guideline for ethical review of animal welfare). The study was designed, performed and reported in accordance with the ARRIVE 2.0 guidelines.

Animals were randomly allocated to two arms of five on the day of inoculation using a random number sequence generated in Microsoft Excel after stratification by body weight, and the cages were randomly positioned on the rack. A group size of five was chosen on the basis of previous subcutaneous xenograft studies of comparable design and the 3Rs principle of reduction. No formal a priori power calculation was performed. All inoculated animals were included in the analysis; no animal was excluded, and no data points were removed. Tumor measurement and the acquisition and quantification of immunohistochemical images were performed by an investigator blinded to group allocation, with samples coded before histological processing. The primary outcome was tumor volume on day 25. Secondary outcomes were terminal tumor weight and the immunoreactivity of EP300, Ki-67, CD163 and p-STAT3, expressed as mean optical density.

Each mouse received a right dorsal flank injection of 5×10^6 CAL-27-shNC or CAL-27-shEP300 cells delivered in 100 µL of PBS pre-mixed with Matrigel at a 1:1 ratio. Caliper measurements were obtained every third day from day 7 onward, and tumor volume was calculated using the formula $V = 0.5 \times L \times W^2$, in which L is the longest diameter and W is the perpendicular short axis. General health, behavior and body weight were monitored daily. Predefined humane endpoints were a tumor volume above 2000 mm^3, tumor ulceration, or a body weight loss of more than 20%. No animal met any of these criteria, and no adverse events were observed.

The experiment was terminated on day 25 when mice were deeply anesthetized with pentobarbital sodium (50 mg/kg, i.p.; HY-B1207A, MedChemExpress, Monmouth Junction, NJ, USA) and sacrificed by decapitation as a secondary physical method. Tumors were then excised, photographed, weighed, and placed in 4% paraformaldehyde pending histology.

Immunohistochemistry

Paraffin blocks prepared from the fixed tumors were sectioned at 4 µm. Sections underwent xylene deparaffinization and graded-ethanol rehydration, after which epi-

topes were retrieved by heating in citrate buffer (pH 6.0, G1202, Servicebio, Wuhan, China). Endogenous peroxidase was quenched by incubation in 3% hydrogen peroxide (10011218, Sinopharm Chemical Reagent, Shanghai, China) for 10 min, and sections were blocked with 3% BSA (GC305010, Servicebio, Wuhan, China) for 30 min to limit non-specific binding. Sections were then incubated overnight at 4 °C with antibodies against EP300 (1:200, A13016, Abclonal Technology, Wuhan, China), Ki-67 (1:200, A20018, Abclonal Technology), CD163 (1:200, A26411PM, Abclonal Technology) and p-STAT3 Tyr705 (1:200, GB150001-100, Servicebio), followed by incubation with an HRP-conjugated secondary reagent (GB23303, Servicebio) for 30 min at room temperature. Color was developed in 3,3′-diaminobenzidine (G1212, Servicebio, Wuhan, China), with hematoxylin (G1004, Servicebio, Wuhan, China) used as the counterstain. Five randomly selected fields per section were captured at 200× magnification, and a defined region within each field was subsequently re-imaged at 400× magnification using an E100 microscope (Nikon Corporation, Tokyo, Japan). ImageJ (version 1.54b, National Institutes of Health, Bethesda, MD, USA) was used to calculate the mean optical density, with values normalized to those of the shNC group. Mean optical density reflects the overall intensity of positive staining within the field and does not discriminate between a change in the number of positive cells and a change in the amount of antigen per cell. The immunohistochemical data are therefore reported as immunoreactivity rather than as cell counts.

Statistical Analysis

Each *in vitro* experiment was repeated independently three times, and five animals per arm were used *in vivo*. For all *in vivo* analyses, the individual mouse was considered the experimental unit, and all animals were included in the analysis. No data points were excluded. Data are expressed as mean ± standard deviation. GraphPad Prism (version 10.1.2, GraphPad Software, Boston, MA, USA) was used for all statistical analyses. Comparisons between two groups were performed using an unpaired two-tailed Student's *t*-test, whereas datasets involving three or more groups were analyzed using one-way ANOVA followed by Tukey's post hoc procedure. Tumor growth curves were evaluated using two-way repeated-measures ANOVA. The Shapiro-Wilk test was applied to assess normality before parametric testing. Significance was set at $p < 0.05$.

Results

EP300 is Upregulated in the OSCC Cell Line CAL-27

To determine whether EP300 is dysregulated in OSCC, we first compared its expression between the human OSCC cell line CAL-27 and normal HOK. qRT-PCR revealed that EP300 mRNA was significantly higher in CAL-27 cells than in HOK cells ($p < 0.001$, Fig. 1A). Consistently, Western blotting showed a markedly stronger EP300 band in CAL-27 cells (Fig. 1B), and densitometric analysis normalized to GAPDH confirmed a significant increase in EP300 protein relative to HOK cells ($p < 0.001$, Fig. 1C). These data indicate that EP300 is upregulated in OSCC cells at both the transcriptional and translational levels, prompting us to investigate its functional role in OSCC progression.

Establishment of EP300 Knockdown and Overexpression Models in CAL-27 Cells

To manipulate EP300 expression, CAL-27 cells were transduced with an EP300-targeting short hairpin RNA (shEP300) or a scrambled control (shNC), or transfected with the pcDNA3.1-EP300 overexpression plasmid (OE-EP300) or the empty vector. Relative to shNC, shEP300 reduced EP300 mRNA ($p < 0.001$, Fig. 1D) and EP300 protein ($p < 0.001$, Fig. 1E,F). Conversely, OE-EP300 increased EP300 mRNA ($p < 0.001$, Fig. 1G) and EP300 protein ($p < 0.01$, Fig. 1H,I) compared with the vector control. The knockdown and overexpression efficiencies were therefore satisfactory, and these transfected cells were used in all subsequent experiments.

EP300 Expression is Associated With JAK2/STAT3 Activation in OSCC Cells

Western blotting of the four experimental groups (shNC, shEP300, vector and OE-EP300) showed that EP300 silencing significantly suppressed the phosphorylation of JAK2 (p-JAK2) and STAT3 (p-STAT3) (Fig. 2A). Quantification revealed that the p-JAK2/JAK2 and p-STAT3/STAT3 ratios were significantly lower in shEP300 cells than in shNC cells (both $p < 0.001$, Fig. 2B). In contrast, EP300 overexpression increased the p-JAK2/JAK2 and p-STAT3/STAT3 ratios ($p < 0.001$ for p-JAK2/JAK2 and $p < 0.01$ for p-STAT3/STAT3, Fig. 2B). To distinguish a change in phosphorylation from a change in total protein expression, total JAK2 and total STAT3 were additionally quantified relative to GAPDH in the same lysates. Neither differed significantly among the four groups (all $p > 0.05$, Fig. 2B). The changes in the p-JAK2/JAK2 and p-STAT3/STAT3 ratios therefore reflect altered phosphorylation of JAK2 and STAT3 rather than altered abundance of the corresponding total proteins. Thus, EP300 abundance is associated with the phosphorylation of JAK2 and STAT3 in OSCC cells.

To confirm that the downstream effects of EP300 could be uncoupled pharmacologically, OE-EP300 cells were treated with the selective STAT3 inhibitor Stattic or an equal volume of DMSO. Stattic significantly reduced the p-STAT3/STAT3 ratio compared with the DMSO-treated group, without completely abolishing STAT3 phosphorylation ($p < 0.001$, Fig. 2C), confirming substantial but incomplete inhibition of STAT3 phosphorylation in the EP300-overexpressing background and supporting the rescue design used below.

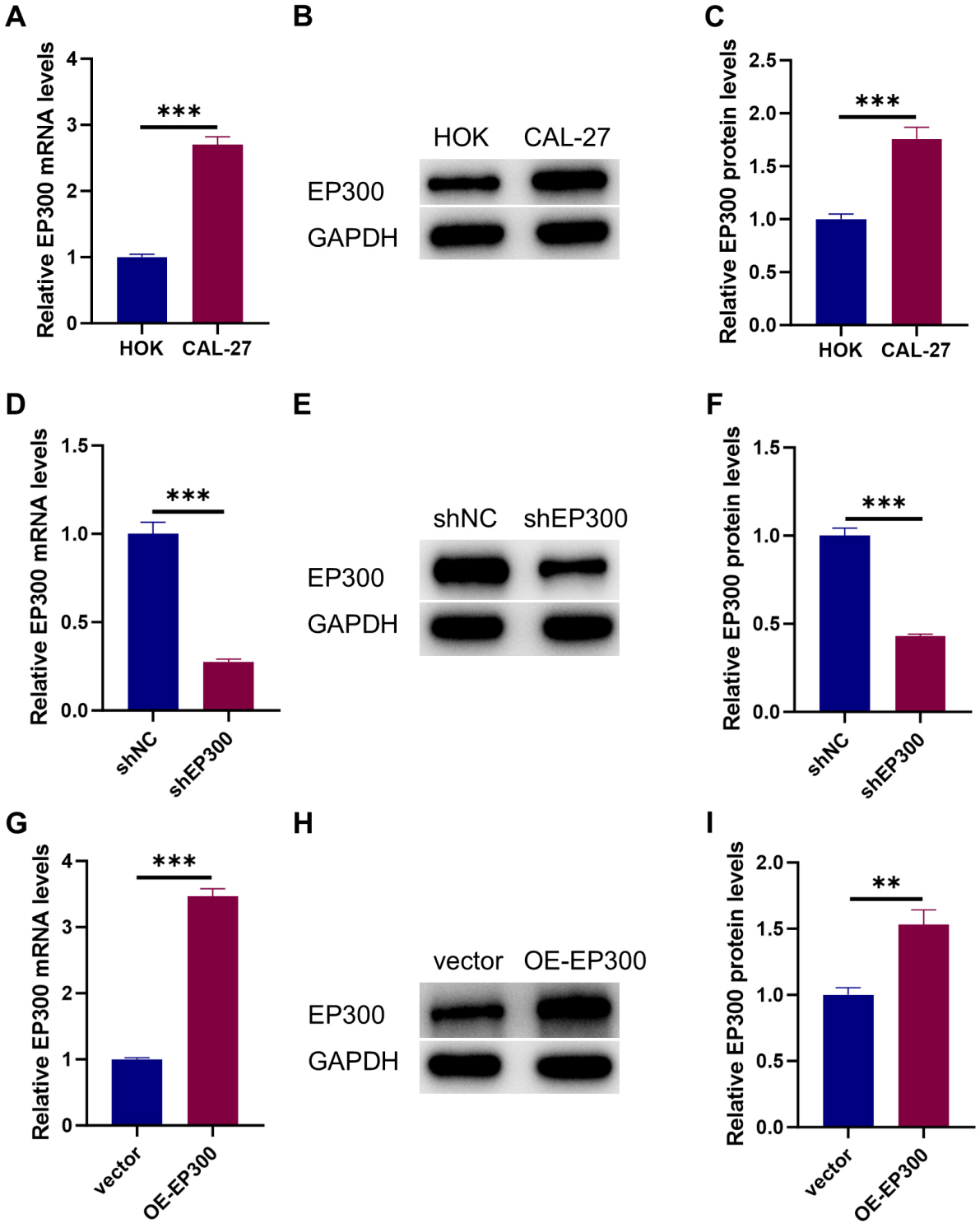


Fig. 1. EP300 is upregulated in OSCC cells and is efficiently manipulated in CAL-27 cells. (A) Relative EP300 mRNA levels in HOK and CAL-27 cells determined by qRT-PCR. (B) Representative Western blotting of EP300 in HOK and CAL-27 cells. (C) Densitometric quantification of (B). (D–F) Validation of EP300 knockdown in CAL-27 cells transduced with shNC or shEP300, including (D) qRT-PCR, (E) representative blot, (F) quantification. (G–I) Validation of EP300 overexpression in CAL-27 cells transfected with an empty vector or OE-EP300, including (G) qRT-PCR, (H) representative blot, (I) quantification. Data are presented as mean ± SD from three independent experiments. $^{**}p < 0.01$, $^{***}p < 0.001$. OSCC, oral squamous cell carcinoma; HOK, human oral keratinocytes; qRT-PCR, quantitative reverse transcription polymerase chain reaction; shNC, negative control short hairpin RNA; SD, standard deviation.

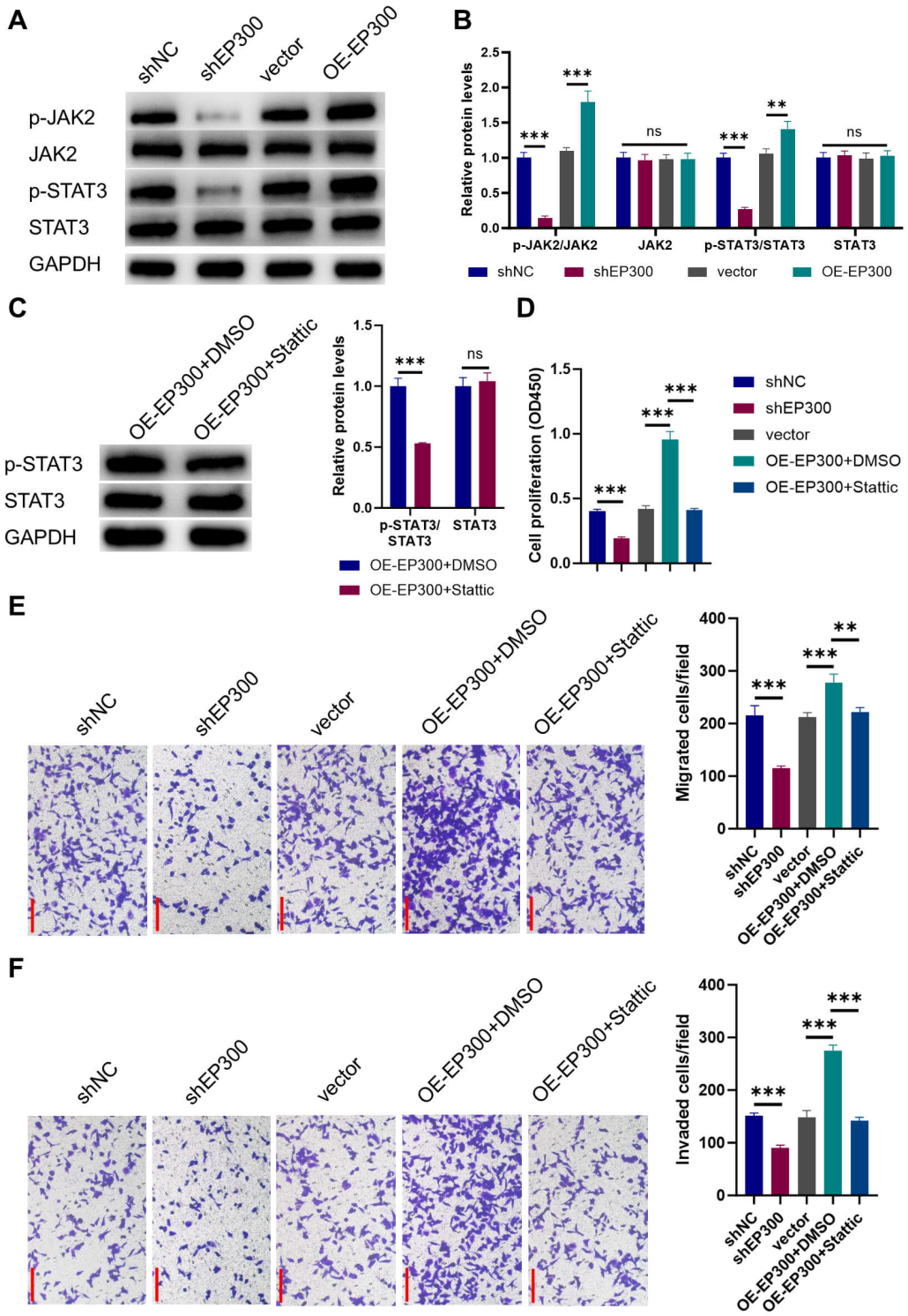


Fig. 2. EP300 expression is associated with JAK2/STAT3 activation and promotes the malignant phenotype of CAL-27 cells, which is attenuated by STAT3 inhibition. (A) Representative Western blots of p-JAK2, total JAK2, p-STAT3 and total STAT3 in shNC, shEP300, vector and OE-EP300 cells. (B) Quantification of p-JAK2/JAK2 and p-STAT3/STAT3 ratios from (A). Total JAK2 and total STAT3 normalized to GAPDH are shown in the same panel. (C) Western blotting and quantification of p-STAT3/STAT3 and total STAT3 in OE-EP300 cells treated with DMSO or Stattic (5 μM). (D) Cell viability at 48 h measured by CCK-8. (E) Transwell migration assay (24 h) with representative images and quantification of migrated cells per field (scale bar = 100 μm). (F) Matrigel-coated Transwell invasion assay (48 h) with representative images and quantification of invaded cells per field. Scale bar = 100 μm. Data are expressed as mean ± SD, n = 3. $^{**}p < 0.01$, $^{***}p < 0.001$; ns, not significant. JAK2, Janus kinase 2; STAT3, signal transducer and activator of transcription 3; GAPDH, glyceraldehyde-3-phosphate dehydrogenase; DMSO, Dimethyl sulfoxide; CCK-8, Cell Counting Kit-8.

STAT3 Inhibition Attenuates the EP300-Associated Increase in OSCC Cell Viability, Migration and Invasion

CCK-8 assays (Fig. 2D) performed at 48 h showed that EP300 knockdown significantly reduced cell viability compared with shNC ($p < 0.001$), whereas EP300 overexpression markedly enhanced cell viability relative to the vector control ($p < 0.001$). Importantly, Stattic abrogated this proliferative advantage, returning the OD450 of OE-EP300 cells to a level comparable to the vector control ($p < 0.001$ vs OE-EP300 + DMSO, Fig. 2D). The number of migrated cells per field decreased in the shEP300 group ($p < 0.001$) and increased in the OE-EP300 + DMSO group ($p < 0.001$). Stattic treatment reduced the number of migrated OE-EP300 cells to a level comparable to that in the vector control group ($p < 0.01$, Fig. 2E). Similarly, Matrigel invasion assays showed fewer invaded cells per field in the shEP300 group than in the shNC group ($p < 0.001$), and more in the OE-EP300 + DMSO group than in the vector group ($p < 0.001$), with Stattic treatment reducing the number of invaded cells ($p < 0.001$ vs OE-EP300 + DMSO, Fig. 2F). These data indicate that EP300 overexpression is associated with increased viability and with greater numbers of migrated and invaded cells, and that pharmacological inhibition of STAT3 reverses these increases.

EP300-Overexpressing OSCC Cells Increase M2-Associated Marker Expression in THP-1-Derived Macrophages Through Soluble Factors

We next examined whether EP300 in tumor cells influences macrophage phenotype through soluble mediators. To limit the influence of the proliferative difference between groups on conditioned-medium composition, donor cultures were matched for confluence, and conditioned medium was collected in a fixed volume over a fixed 24-h interval. Western blotting showed that CM from EP300-silenced cells markedly reduced the M2-associated markers CD163 and Arg-1 in macrophages (both $p < 0.001$), whereas CM from EP300-overexpressing cells increased CD163 and Arg-1 (both $p < 0.001$, Fig. 3). IL-4 plus IL-13 produced the strongest induction, as expected for a positive control. In contrast, the M1 marker CD86 remained essentially unchanged across all groups ($p > 0.05$, Fig. 3), indicating that the effect of EP300-driven paracrine signaling was largely restricted to M2-associated markers. The p-STAT3/STAT3 ratio in macrophages paralleled the M2-associated marker profile, decreasing with shEP300 CM ($p < 0.001$) and increasing with OE-EP300 CM ($p < 0.001$, Fig. 3), suggesting that STAT3 is also activated in recipient macrophages and may mediate this response. Total STAT3 normalized to GAPDH did not differ significantly among the groups ($p > 0.05$), indicating that the change in the p-STAT3/STAT3 ratio in macrophages likewise reflects a difference in STAT3 phosphorylation rather than in total STAT3 expression.

STAT3 Inhibition Attenuates CM-Induced Increase in M2-Associated Marker Expression in Macrophages

Stattic substantially suppressed STAT3 activation in macrophages, significantly lowering the p-STAT3/STAT3 ratio compared with that in the OE-EP300 CM plus DMSO group ($p < 0.001$, Fig. 4). Conditioned medium from EP300-overexpressing cells increased the macrophage p-STAT3/STAT3 ratio relative to vector CM ($p < 0.01$, Fig. 4). OE-EP300 CM increased CD163 and Arg-1 (both $p < 0.001$). Co-treatment with Stattic largely abolished this induction, returning CD163 and Arg-1 to levels comparable to the vector CM plus DMSO control group (both $p < 0.001$, Fig. 4). These results indicate that inhibition of STAT3 in macrophages reverses the increase in M2-associated markers induced by conditioned medium from EP300-overexpressing OSCC cells.

EP300 Knockdown Suppresses Tumor Growth and Reduces CD163 Immunoreactivity In Vivo

We validated these findings in a subcutaneous xenograft model. BALB/c nude mice (female, 6 weeks old, n = 5 per group, randomly allocated) received 5×10^6 CAL-27-shNC or CAL-27-shEP300 cells in the right dorsal flank, and tumor dimensions were recorded every 3 days. All tumors excised on day 25 are shown in Fig. 5A. Those derived from shEP300 cells were consistently smaller than those from shNC cells. Growth curves diverged progressively from day 13 onward, and on day 25, the mean tumor volume in the shEP300 group was significantly reduced compared with that in the shNC group ($p < 0.001$). Terminal tumor weight was correspondingly reduced ($p < 0.001$, Fig. 5B). Immunohistochemical analysis of the xenografts confirmed efficient EP300 silencing, with markedly weaker nuclear EP300 staining in shEP300 tumors than in shNC tumors ($p < 0.001$, Fig. 5C). Consistent with the reduced tumor burden, the proliferation index Ki-67 was decreased in shEP300 tumors ($p < 0.001$, Fig. 5D). Importantly, CD163 immunoreactivity was reduced in shEP300 tumors ($p < 0.001$, Fig. 5E), and p-STAT3 staining was also reduced ($p < 0.001$, Fig. 5F). Together, these *in vivo* data corroborate the *in vitro* findings and indicate that EP300 knockdown suppresses xenograft growth, accompanied by reduced p-STAT3 and CD163 immunoreactivity within the tumor microenvironment.

Discussion

In the present study, we found that EP300 was expressed at higher levels in the OSCC cell line CAL-27 than in normal HOK, and that manipulating EP300 in CAL-27 cells altered JAK2/STAT3 phosphorylation, proliferation, and the number of cells traversing Transwell membranes, in a direction consistent with a tumor-promoting role. Conditioned medium from EP300-overexpressing CAL-27 cells increased CD163 and Arg-1 in THP-1-derived

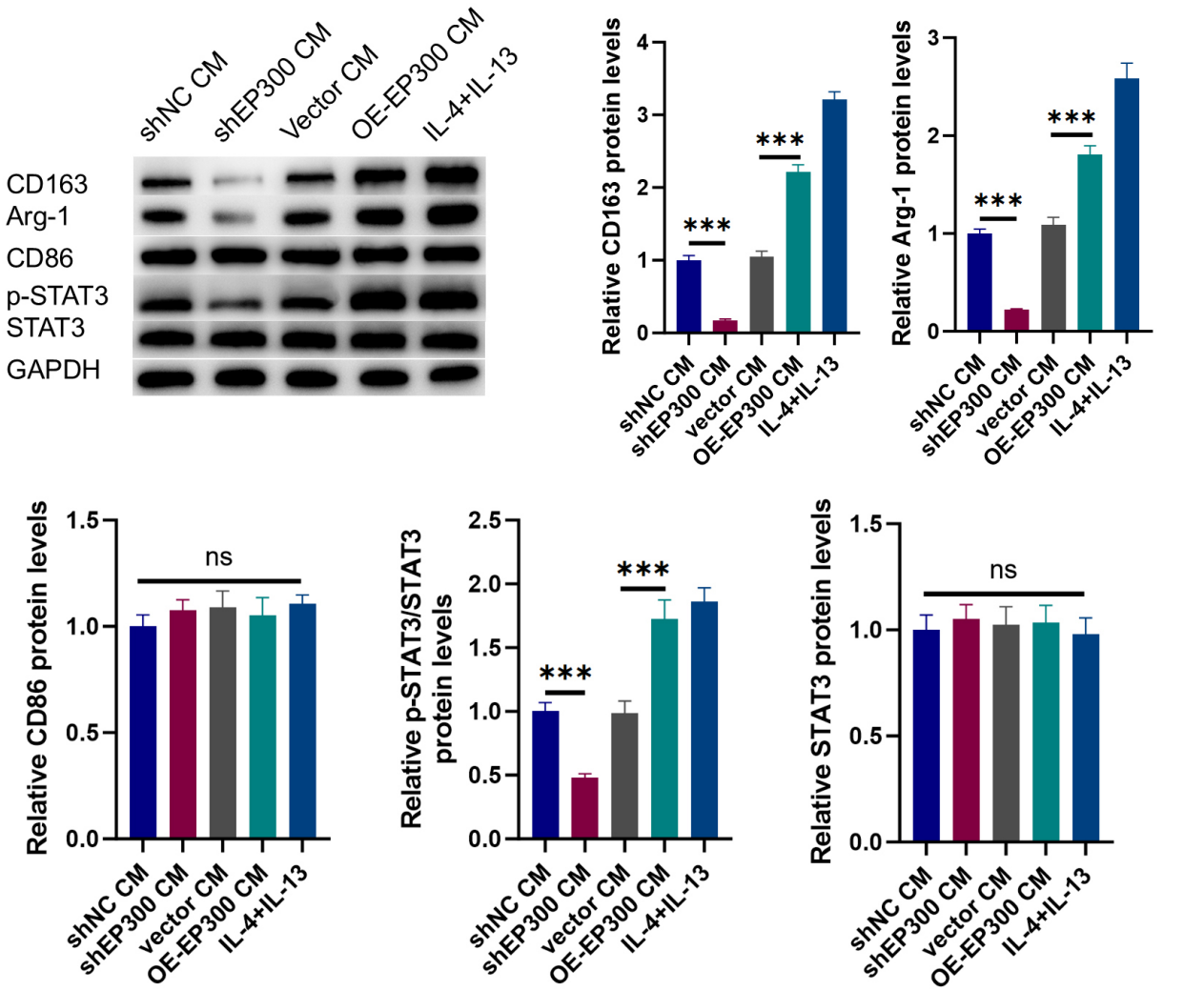


Fig. 3. Conditioned medium from EP300-overexpressing OSCC cells increases M2-associated marker expression in THP-1-derived macrophages. Representative Western blots and densitometric quantification of CD163, Arg-1, CD86, p-STAT3 and total STAT3 in PMA-differentiated THP-1 macrophages exposed to conditioned medium from shNC, shEP300, vector or OE-EP300 CAL-27 cells, or to IL-4 (20 ng/mL) plus IL-13 (20 ng/mL) as a positive control. Conditioned medium was collected in a fixed volume over a fixed 24-h interval from donor cultures matched for confluence and diluted with an equal volume of fresh complete medium before use. Data are expressed as mean ± SD, n = 3. ***$p < 0.001$; ns, not significant. THP-1, Tohoku Hospital Pediatrics-1; CD163, cluster of Differentiation 163; Arg-1, Arginase 1; PMA, phorbol 12-myristate 13-acetate; IL-4, Interleukin-4.

macrophages without a detectable change in CD86, and this effect was largely attenuated by pharmacological inhibition of STAT3 in the recipient macrophages. In a subcutaneous xenograft model, EP300 knockdown reduced tumor volume and weight, accompanied by lower Ki-67, p-STAT3 and CD163 immunoreactivity. Taken together, these observations are compatible with a model in which EP300 supports OSCC growth in association with increased JAK2/STAT3 phosphorylation and is associated with an M2-associated macrophage marker profile. We emphasize, however, that several links in this model remain correlative, as detailed below.

EP300 (p300) and its paralogue CBP are transcriptional coactivators with intrinsic histone acetyltransferase activity, and their role in cancer is context-dependent rather than uniformly oncogenic or tumor-suppressive [35]. Inactivating EP300 mutations have been reported in squamous carcinomas, including head and neck squamous cell carcinoma [31], which at first appears difficult to reconcile with the tumor-promoting phenotype observed here. Two considerations are relevant. First, mutational inactivation in a subset of tumors and overexpression in others are not mutually exclusive; second, the functional consequence of EP300 loss may depend on the co-occurring genetic background [31,36]. Our conclusions are based on a single cell line with an intact EP300 locus and should not be generalized to EP300-mutant OSCC. Determining whether EP300 dependency is associated with EP300 mutational status in

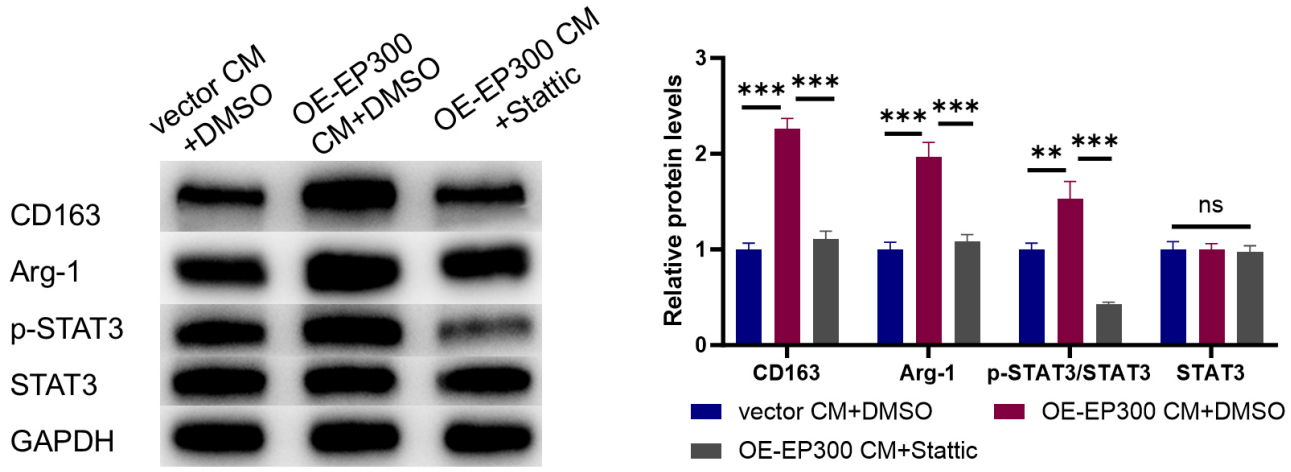


Fig. 4. STAT3 inhibition attenuates conditioned medium-induced increase in M2-associated marker expression. Representative Western blots and quantification of CD163, Arg-1, p-STAT3 and total STAT3 in THP-1-derived macrophages treated with vector CM plus DMSO, OE-EP300 CM plus DMSO, or OE-EP300 CM plus Stattic (5 μM). Conditioned medium was collected in a fixed volume over a fixed 24-h interval from donor cultures matched for confluence and diluted with an equal volume of fresh complete medium before use. Data are expressed as mean ± SD, n = 3. $^{**}p < 0.01$, $^{***}p < 0.001$; ns, not significant; CM, conditioned medium.

OSCC will require analysis of a larger panel of cell lines and of clinical specimens, which was beyond the scope of the present study.

The link we observed between EP300 and JAK2/STAT3 activity is a regulatory relationship rather than a demonstrated direct interaction. We did not perform chromatin immunoprecipitation, acetylation-specific immunoblotting or co-immunoprecipitation, and therefore cannot distinguish between transcriptional regulation of pathway components by EP300 and post-translational modification of the pathway itself. It has previously been reported that p300 acetylates STAT3 at Lys685 and that this modification contributes to STAT3 dimerization and transcriptional activity [34]. Whether such a mechanism operates in OSCC cells, and whether it accounts for the change in p-JAK2 that we observed upstream of STAT3, remains to be tested. The simultaneous change in p-JAK2 suggests that at least part of the effect occurs at or above the level of JAK2, but our data do not identify the responsible node. Importantly, no loss-of-function or rescue experiment targeting JAK2 itself was performed. We did not inhibit, silence or re-express JAK2, and therefore cannot conclude that JAK2 constitutes a necessary link between EP300 and STAT3. Pharmacological inhibition or silencing of JAK2, with assessment of whether the EP300-associated changes in p-STAT3 and the malignant phenotype are abolished, would be required to test this possibility.

Constitutive or persistent STAT3 activation is frequently observed in HNSCC, including OSCC, and has been implicated in tumor-cell proliferation, invasion, and immune evasion [27,37]. Our rescue experiments are consistent with STAT3 acting downstream of EP300 in this setting, since Stattic reversed the proliferative, migratory and invasive advantage conferred by EP300 overexpression. It should be noted that Stattic is a small-molecule inhibitor with recognized off-target reactivity [38,39], and it reduced p-STAT3 only partially rather than abolishing it. A genetic approach, such as STAT3 knockdown or expression of a dominant-negative STAT3, would provide stronger evidence for a strict dependency and would be a logical next step. A further limitation of the rescue design is that a vector plus Stattic arm was not included. Stattic was applied only to EP300-overexpressing cells, so a non-specific contribution of the compound to the reduction in viability, migration and invasion cannot be formally excluded. We note that, in each assay, the values obtained with OE-EP300 plus Stattic returned to the level of the vector control rather than falling below it, which would not be expected with generalized cytotoxicity. However, this is an indirect inference, and a vector plus Stattic control together with genetic STAT3 silencing would be required to establish that the reversal is specific to the EP300-driven signal. The same consideration applies to the macrophage experiments in Fig. 4.

With respect to the tumor-macrophage interaction, our conditioned-medium experiments indicate that EP300-overexpressing OSCC cells release one or more soluble factors capable of increasing M2-associated markers in macrophages, and that inhibition of STAT3 in the macrophage reverses this response. A principal limitation of this study is that the responsible soluble mediator or mediators were not identified. Conditioned medium is a complex mixture, and the observed effect could be produced by cytokines, growth factors, metabolites or extracellular vesicles, either individually or in combination. Factors including IL-6, IL-10, CSF-1, and VEGF have been

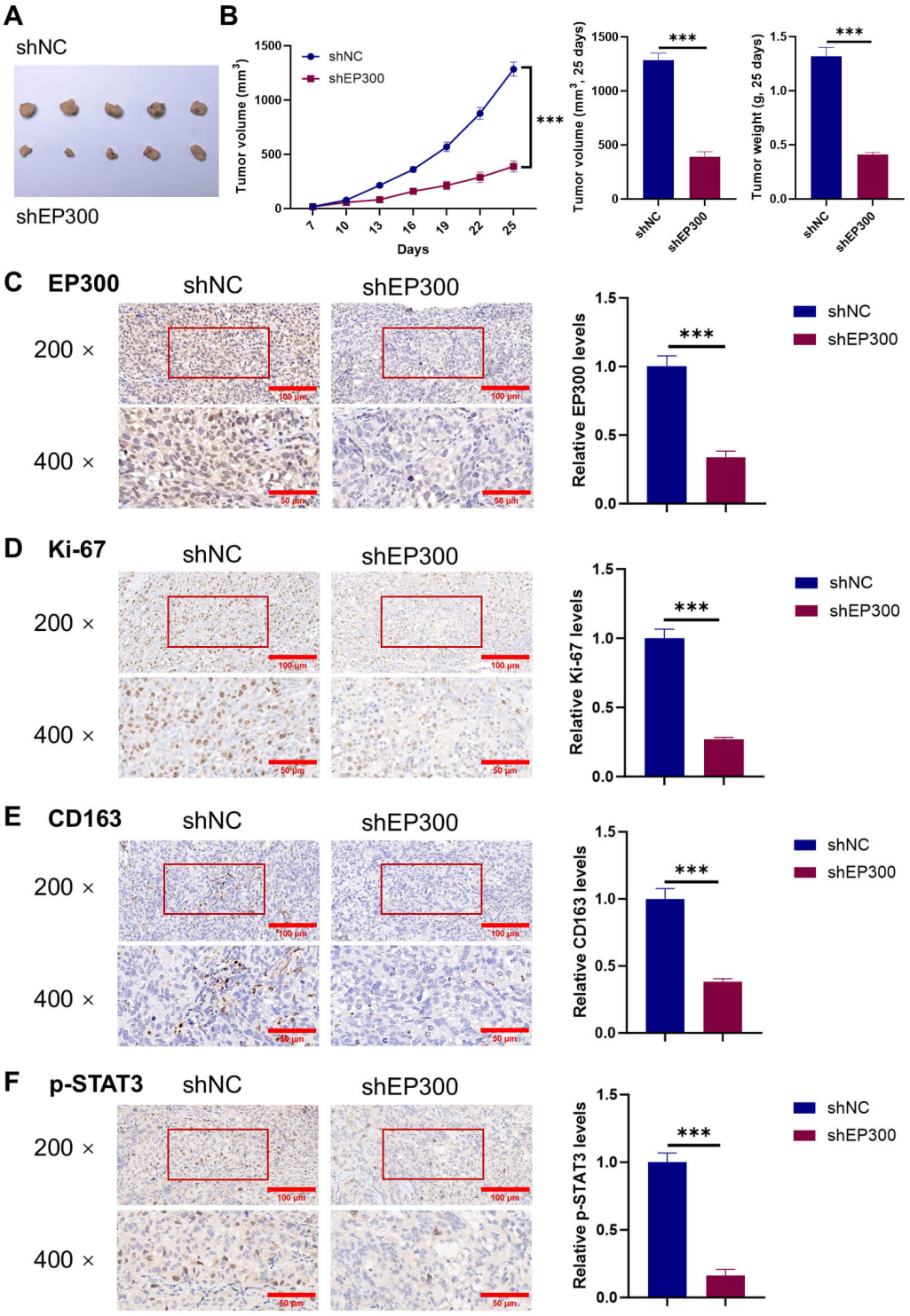


Fig. 5. EP300 knockdown suppresses xenograft growth and reduces CD163 immunoreactivity *in vivo*. (A) Photographs of all subcutaneous tumors excised on day 25 from mice inoculated with CAL-27-shNC or CAL-27-shEP300 cells (n = 5 per group). (B) Tumor growth curves, terminal tumor volume and tumor weight at day 25. (C–F) Representative immunohistochemical images (200× and 400×) and quantification of (C) EP300, (D) Ki-67, (E) CD163 and (F) p-STAT3 in xenograft sections. For each marker, the upper row shows the 200× field and the lower row the corresponding 400× field. The red rectangle in each 200× image delineates the region shown at 400×. Scale bars = 100 μm (200×) and 50 μm (400×). n = 5 mice per group; data are expressed as mean ± SD. ***$p < 0.001$. Immunohistochemical signals were quantified as mean optical density and are therefore reported as immunoreactivity rather than as numbers of positive cells.

implicated in the development or maintenance of tumor-supportive macrophage states, with IL-6 and IL-10 providing the clearest evidence for direct JAK/STAT3-dependent polarization [40]. However, we did not measure these factors, and therefore make no claim as to which molecule mediates the effect described here. Cytokine array or targeted ELISA profiling of the conditioned media, followed by neutralizing-antibody or recombinant-protein add-back experiments, would be required to address this gap. Until such experiments are performed, the paracrine step in our model should be regarded as demonstrated in principle but undefined in identity.

A further caveat concerns the conditioned medium itself. EP300 manipulation changed CAL-27 proliferation, and any difference between preparations could therefore reflect the number of cells that produced the medium rather than a change in what each cell secretes. Donor cultures were matched for confluence and medium was collected in a fixed volume over a fixed interval, which constrains but does not eliminate this possibility, since we did not enumerate viable donor cells at the point of harvest, measure the total protein content of the preparations, or apply the media across a range of donor-cell equivalents. A concentration-driven explanation is therefore not formally excluded by our data. Quantification of a candidate mediator in donor-cell-normalized medium, together with dose-matched recombinant add-back, would be needed to establish whether EP300 alters per-cell secretory output rather than merely the number of secreting cells. The paracrine effect reported here should accordingly be interpreted as a property of conditioned medium from EP300-manipulated cultures collected under matched conditions, rather than as evidence of a demonstrated change in per-cell secretion.

Also, the macrophage marker experiments used human THP-1-derived macrophages exposed to human OSCC conditioned medium, whereas the CD163 signal scored in the xenografts derives from host murine cells recruited to a human tumor. The two readouts are therefore not directly equivalent, and the *in vivo* immunohistochemistry should be interpreted as a correlate of the *in vitro* finding rather than as its confirmation in the same cellular system. Cross-species differences in macrophage polarization markers are well recognized, and Arg-1 behaves differently in murine and human macrophages in particular [41], which is one reason we restricted the *in vivo* analysis to CD163. In addition, BALB/c nude mice lack functional T cells, so any contribution of adaptive immunity to the phenotype could not be assessed, and the myeloid compartment in this model does not fully recapitulate the immune context of human OSCC. A syngeneic murine OSCC model, an orthotopic tongue model, or a humanized-mouse system would be needed to establish whether the same tumor-macrophage circuit operates *in vivo*, and macrophage depletion would be required to test whether M2-associated TAMs contribute causally to the observed difference in tumor growth. A further limitation concerns the quantification of the immunohistochemical data. Staining was assessed as mean optical density, which reports the overall intensity of the positive signal within a field but cannot distinguish a reduction in the number of CD163-positive macrophages from a reduction in CD163 expression per cell. Our *in vivo* data therefore support a decrease in CD163 immunoreactivity, and should not be read as a direct demonstration of reduced macrophage infiltration. Counting of CD163-positive cells per field, co-staining with a pan-macrophage marker such as F4/80, or flow-cytometric quantification of tumor-infiltrating myeloid populations would be required to establish whether the density of infiltrating macrophages is genuinely altered. As the present study stands, the reduction in tumor burden and the reduction in CD163 immunoreactivity are concurrent observations, and we do not claim a causal relationship between them.

Only one OSCC cell line was examined, so cell-line-specific effects cannot be excluded. We did not analyze clinical OSCC specimens or public expression datasets; consequently, the clinical relevance of EP300 expression in OSCC cannot be addressed by the present data. The CCK-8 assay was read at a single time point, which captures a difference in viability but not the shape of the growth curve. Another limitation concerns the Transwell assays. EP300 manipulation altered cell viability, and Stattic may itself affect cell state, so the numbers of migrated and invaded cells cannot be attributed exclusively to changes in intrinsic motility or invasiveness. Equal numbers of cells were seeded into each insert, and cells were serum-starved for 12 h and loaded in serum-free medium, limiting proliferation within the upper chamber during the assay. Nevertheless, we did not block proliferation with mitomycin C, shorten the incubation, or normalize the counts to viable cell number, and a contribution of differences in proliferation or survival, particularly over the 48-h invasion assay, therefore cannot be excluded. Transwell data should accordingly be interpreted as differences in the number of cells traversing the membrane rather than as independent measures of migratory and invasive capacity. The xenograft model was subcutaneous rather than orthotopic and did not include a metastasis endpoint, so the migration and invasion phenotypes observed *in vitro* were not tested *in vivo*. Finally, our overexpression experiments used transient transfection, which may not reflect the effect of chronic, physiological changes in EP300 abundance.

Notwithstanding these limitations, the observations reported here may have translational relevance. Catalytic and bromodomain inhibitors of p300/CBP have been developed, and some have entered clinical evaluation in other tumor types [42]. If the association between EP300 activity and STAT3-associated macrophage skewing described here is confirmed in more physiologically relevant models, it would provide a rationale for evaluating such agents, alone or in combination with STAT3-directed or macrophage-

directed strategies, in preclinical OSCC studies. We regard this as a hypothesis generated by the present work rather than a conclusion directly supported by the available evidence.

Conclusions

In summary, our data indicate that EP300 is associated with an enhanced malignant phenotype in CAL-27 OSCC cells, accompanied by increased JAK2/STAT3 signaling; that conditioned medium from EP300-overexpressing OSCC cells increases M2-associated markers in human macrophages, an effect that is reversed by pharmacological inhibition of STAT3; and that EP300 knockdown reduces xenograft growth with a concomitant decrease in Ki-67, p-STAT3 and CD163 immunoreactivity. Identification of the mediating soluble factor and validation in immunocompetent, species-matched models are the necessary next steps.

Availability of Data and Materials

The data that support the findings of this study are available from the corresponding author upon reasonable request.

Author Contributions

WWH, JSY and SM designed the research study. WLL, JSY and WWH performed the research. WWH, WLL and SM analyzed the data. WWH drafted the initial manuscript. All authors contributed to important editorial changes in the manuscript. All authors read and approved the final manuscript. All authors have participated sufficiently in the work and agreed to be accountable for all aspects of the work.

Ethics Approval and Consent to Participate

All animal experiments were reviewed and approved by the Experimental Animal Welfare and Ethics Committee of Hebei North University (approval No. HBNU20240622143, approved on 17 June 2024). All procedures complied with the ARRIVE Guidelines 2.0.

Acknowledgment

Not applicable.

Funding

This research was supported by the 2025 Program of Research Projects in Traditional Chinese Medicine Sciences (Grant No.2025385).

Conflict of Interest

The authors declare no conflict of interest.

References

[1] Tan Y, Wang Z, Xu M, Li B, Huang Z, Qin S, et al. Oral squamous cell carcinomas: state of the field and emerging directions. International Journal of Oral Science. 2023; 15: 44. https://doi.org/10.1038/s41368-023-00249-w

[2] Mohamad I, Glaun MDE, Prabhash K, Busheri A, Lai SY, Noronha V, et al. Current Treatment Strategies and Risk Stratification for Oral Carcinoma. American Society of Clinical Oncology Educational Book. American Society of Clinical Oncology. Annual Meeting. 2023; 43: e389810. https://doi.org/10.1200/EDBK_389810

[3] Wang Y, Yang T, Gan C, Wang K, Sun B, Wang M, et al. Temporal and spatial patterns of recurrence in oral squamous cell carcinoma, a single-center retrospective cohort study in China. BMC Oral Health. 2023; 23: 679. https://doi.org/10.1186/s12903-023-03204-7

[4] Alqutub S, Alqutub A, Bakhshwin A, Mofti Z, Alqutub S, Alkhamesi AA, et al. Histopathological predictors of lymph node metastasis in oral cavity squamous cell carcinoma: a systematic review and meta-analysis. Frontiers in Oncology. 2024; 14: 1401211. https://doi.org/10.3389/fonc.2024.1401211

[5] Nathan CA, Khandelwal AR, Wolf GT, Rodrigo JP, Mäkitie AA, Saba NF, et al. TP53 mutations in head and neck cancer. Molecular Carcinogenesis. 2022; 61: 385–391. https://doi.org/10.1002/mc.23385

[6] Cheng H, Jiang M, Kim S, Moshiri A, Dar MS, Akhtar J, et al. Uncovering chromatin factor landscapes in head and neck squamous cell carcinoma. Oral Oncology. 2025; 170: 107687. https://doi.org/10.1016/j.oraloncology.2025.107687

[7] Ngan HL, Law CH, Choi YCY, Chan JYS, Lui VWY. Precision drugging of the MAPK pathway in head and neck cancer. NPJ Genomic Medicine. 2022; 7: 20. https://doi.org/10.1038/s41525-022-00293-1

[8] Li J, Li S, Shu M, Hu W. Unravelling the heterogeneity of oral squamous cell carcinoma by integrative analysis of single-cell and bulk transcriptome data. Journal of Cellular and Molecular Medicine. 2024; 28: e18108. https://doi.org/10.1111/jcmm.18108

[9] Zhi Y, Wang Q, Zi M, Zhang S, Ge J, Liu K, et al. Spatial Transcriptomic and Metabolomic Landscapes of Oral Submucous Fibrosis-Derived Oral Squamous Cell Carcinoma and its Tumor Microenvironment. Advanced Science. 2024; 11: e2306515. https://doi.org/10.1002/advs.202306515

[10] Hu C, Zhang Y, Wu C, Huang Q. Heterogeneity of cancer-associated fibroblasts in head and neck squamous cell carcinoma: opportunities and challenges. Cell Death Discovery. 2023; 9: 124. https://doi.org/10.1038/s41420-023-01428-8

[11] Quah HS, Cao EY, Suteja L, Li CH, Leong HS, Chong FT, et al. Single cell analysis in head and neck cancer reveals potential immune evasion mechanisms during early metastasis. Nature Communications. 2023; 14: 1680. https://doi.org/10.1038/s41467-023-37379-y

[12] Zhang H, Qian Y, Zhang Y, Zhou X, Shen S, Li J, et al. Multiomics analysis deciphers intercellular communication regulating oxidative stress to promote oral squamous cell carcinoma progression. NPJ Precision Oncology. 2024; 8: 272. https://doi.org/10.1038/s41698-024-00764-x

[13] Korneenko TV, Pestov NB, Shakhparonov MI, Barlev NA. Microenvironment of Solid Tumors. Frontiers in Bioscience (Landmark Edition). 2025; 30: 36940. https://doi.org/10.31083/FBL36940

[14] Lou J, Luo G, Zhao L, Zhang H. CONSORT article: Single-cell sequencing analysis revealed CMKLR1+ macrophage as a subpopulation of macrophage with tumor-suppressive characteristics in oral squamous cell carcinoma. Medicine. 2024; 103: e39399. https://doi.org/10.1097/MD.0000000000039399

[15] Chohan MH, Perry M, Laurance-Young P, Salih VM, Foey AD. Prognostic Role of CD68+ and CD163+ Tumour-Associated Macrophages and PD-L1 Expression in Oral Squamous Cell Carcinoma: A Meta-Analysis. British Journal of Biomedical Science. 2023; 80: 11065. https://doi.org/10.3389/bjbs.2023.11065

[16] Khumanthem S, Suresh TN, Kattepur AK. Immunohistochemical Study of Tumour-Associated Macrophages Using CD68 and CD163 in Oral Squamous Cell Carcinoma. Indian Journal of Surgical Oncology. 2026; 17: 1052–1056. https://doi.org/10.1007/s13193-025-02391-9

[17] Yamagata Y, Tomioka H, Sakamoto K, Sato K, Harada H, Ikeda T, et al. CD163-Positive Macrophages Within the Tumor Stroma Are Associated With Lymphangiogenesis and Lymph Node Metastasis in Oral Squamous Cell Carcinoma. Journal of Oral and Maxillofacial Surgery: Official Journal of the American Association of Oral and Maxillofacial Surgeons. 2017; 75: 2144–2153. https://doi.org/10.1016/j.joms.2017.03.009

[18] Strizova Z, Benesova I, Bartolini R, Novysedlak R, Cecrdlova E, Foley LK, et al. M1/M2 macrophages and their overlaps - myth or reality? Clinical Science (London, England: 1979). 2023; 137: 1067–1093. https://doi.org/10.1042/CS20220531

[19] Chen S, Saeed AFUH, Liu Q, Jiang Q, Xu H, Xiao GG, et al. Macrophages in immunoregulation and therapeutics. Signal Transduction and Targeted Therapy. 2023; 8: 207. https://doi.org/10.1038/s41392-023-01452-1

[20] Guimarães GR, Maklouf GR, Teixeira CE, de Oliveira Santos L, Tessarollo NG, de Toledo NE, et al. Single-cell resolution characterization of myeloid-derived cell states with implication in cancer outcome. Nature Communications. 2024; 15: 5694. https://doi.org/10.1038/s41467-024-49916-4

[21] Ma RY, Black A, Qian BZ. Macrophage diversity in cancer revisited in the era of single-cell omics. Trends in Immunology. 2022; 43: 546–563. https://doi.org/10.1016/j.it.2022.04.008

[22] Pelaez-Prestel HF, Gonzalez-Martin F, Ras-Carmona A, Rocha A, Cabañas C, Lafuente EM, et al. Oral squamous cell carcinomas drive monocytes into immunosuppressive CD25+CD163+CD206+ macrophages. Oral Oncology. 2024; 159: 107078. https://doi.org/10.1016/j.oraloncology.2024.107078

[23] Wu L, Ye S, Yao Y, Zhang C, Liu W. Oral Cancer Stem Cell-Derived Small Extracellular Vesicles Promote M2 Macrophage Polarization and Suppress CD4+ T-Cell Activity by Transferring UCA1 and Targeting LAMC2. Stem Cells International. 2022; 2022: 5817684. https://doi.org/10.1155/2022/5817684

[24] You Y, Tian Z, Du Z, Wu K, Xu G, Dai M, et al. M1-like tumor-associated macrophages cascade a mesenchymal/stem-like phenotype of oral squamous cell carcinoma via the IL6/Stat3/THBS1 feedback loop. Journal of Experimental & Clinical Cancer Research: CR. 2022; 41: 10. https://doi.org/10.1186/s13046-021-02222-z

[25] Li J, Bao Y, Peng S, Jiang C, Zhu L, Zou S, et al. M2 Macrophages-Derived Exosomal miRNA-23a-3p Promotes the Progression of Oral Squamous Cell Carcinoma by Targeting PTEN. Current Issues in Molecular Biology. 2023; 45: 4936–4947. https://doi.org/10.3390/cimb45060314

[26] Wang P, Tao L, Yu Y, Wang Q, Ye P, Sun Y, et al. Oral squamous cell carcinoma cell-derived GM-CSF regulates PD-L1 expression in tumor-associated macrophages through the JAK2/STAT3 signaling pathway. American Journal of Cancer Research. 2023; 13: 589–601.

[27] Khatoon E, Hegde M, Kumar A, Daimary UD, Sethi G, Bishayee A, et al. The multifaceted role of STAT3 pathway and its implication as a potential therapeutic target in oral cancer. Archives of Pharmacal Research. 2022; 45: 507–534. https://doi.org/10.1007/s12272-022-01398-y

[28] Samad MA, Ahmad I, Hasan A, Alhashmi MH, Ayub A, Al-Abbasi FA, et al. STAT3 Signaling Pathway in Health and Disease. MedComm. 2025; 6: e70152. https://doi.org/10.1002/mco2.70152

[29] Cao W, Zeng Z, Sun J, Chen Y, Kuang F, Luo S, et al. Exosome-derived circ-001422 promotes tumor-associated macrophage M2 polarization to accelerate the progression of glioma. Communications Biology. 2024; 7: 1504. https://doi.org/10.1038/s42003-024-07134-0

[30] Gou P, Zhang W. Protein lysine acetyltransferase CBP/p300: A promising target for small molecules in cancer treatment. Biomedicine & Pharmacotherapy = Biomedecine & Pharmacotherapie. 2024; 171: 116130. https://doi.org/10.1016/j.biopha.2024.116130

[31] Gronkowska K, Robaszkiewicz A. Genetic dysregulation of EP300 in cancers in light of cancer epigenome control - targeting of p300-proficient and -deficient cancers. Molecular Therapy. Oncology. 2024; 32: 200871. https://doi.org/10.1016/j.omton.2024.200871

[32] Tang W, Zhang C, Han L, Fu H, Mao Z, Zhang Y, et al. Curcumin inhibits glycolysis via EP300 in oral squamous cell carcinoma. Scientific Reports. 2026; 16: 11702. https://doi.org/10.1038/s41598-026-44496-3

[33] Wang H, Fu Y, Lin G, Zhang D, Nan X, Liu J, et al. Inhibition of the EP300/Notch Signaling Pathway Regulates Proliferation and Apoptosis in Oral Squamous Cell Carcinoma. Journal of Oral Pathology & Medicine: Official Publication of the International Association of Oral Pathologists and the American Academy of Oral Pathology. 2026; 55: 953–965. https://doi.org/10.1111/jop.70159

[34] Yan H, Tang L, Yuan Z, Zhang Y. The effects of STAT3 acetylation on the transcriptional activity and tumorigenesis. Biochemical Pharmacology. 2025; 240: 117076. https://doi.org/10.1016/j.bcp.2025.117076

[35] Xu L, Xuan H, Shi X. Dysregulation of the p300/CBP histone acetyltransferases in human cancer. Epigenomics. 2025; 17: 193–208. https://doi.org/10.1080/17501911.2024.2447807

[36] George J, Maas L, Abedpour N, Cartolano M, Kaiser L, Fischer RN, et al. Evolutionary trajectories of small cell lung cancer under therapy. Nature. 2024; 627: 880–889. https://doi.org/10.1038/s41586-024-07177-7

[37] Chakraborty R, Khodlan P, Tay A, Liu F. STAT3 interactome predicts presence of proteins that regulate immune system in oral squamous cell carcinoma. Journal of Oral Biosciences. 2024; 66: 67–73. https://doi.org/10.1016/j.job.2024.09.002

[38] Poria DK, Sheshadri N, Balamurugan K, Sharan S, Sterneck E. The STAT3 inhibitor Stattic acts independently of STAT3 to decrease histone acetylation and modulate gene expression. The Journal of Biological Chemistry. 2021; 296: 100220. https://doi.org/10.1074/jbc.RA120.016645

[39] Xia Y, Wang G, Jiang M, Liu X, Zhao Y, Song Y, et al. A Novel Biological Activity of the STAT3 Inhibitor Stattic in Inhibiting Glutathione Reductase and Suppressing the Tumorigenicity of Human Cervical Cancer Cells via a ROS-Dependent Pathway. OncoTargets and Therapy. 2021; 14: 4047–4060. https://doi.org/10.2147/OTT.S313507

[40] Xia T, Zhang M, Lei W, Yang R, Fu S, Fan Z, et al. Advances in the role of STAT3 in macrophage polarization. Frontiers in Immunology. 2023; 14: 1160719. https://doi.org/10.3389/fimmu.2023.1160719

[41] Tanito K, Nii T, Kishimura A, Mori T, Katayama Y. Screening of Human M2 Macrophage-Specific Markers for Preparation of Humanized Inflammation-Triggering Engineered Macrophage (MacTrigger). Biological & Pharmaceutical Bulletin. 2025; 48: 966–971. https://doi.org/10.1248/bpb.b25-00112

[42] Wu X, Zhang X, Tang S, Wang Y. The important role of the histone acetyltransferases p300/CBP in cancer and the promising anticancer effects of p300/CBP inhibitors. Cell Biology and Toxicology. 2025; 41: 32. https://doi.org/10.1007/s10565-024-09984-0